Journal of Power Sources 205 (2012) 377–384

Contents lists available at SciVerse ScienceDirect

Journal of Power Sources

journal homepage: www.elsevier.com/locate/jpowsour

Demonstration of a highly efficient solid oxide fuel cell power system using adiabatic steam reforming and anode gas recirculation

Mike Powell, Kerry Meinhardt, Vince Sprenkle, Larry Chick*, Gary McVay

Pacific Northwest National Laboratory, PO Box 999, Richland, WA 99352, USA

ARTICLE INFO

Article history:
Received 5 December 2011
Received in revised form 13 January 2012
Accepted 14 January 2012
Available online 24 January 2012

Keywords:
Solid oxide fuel cell
Power system
Steam reforming
Distributed generation
High efficiency
Methane

ABSTRACT

Solid oxide fuel cells (SOFCs) are being developed for a wide variety of applications because of their high efficiency over a wide range of power levels. Applications for SOFCs include 1–2 kW residential combined heat and power applications, 100–250 kW systems for distributed generation and grid extension, and megawatt-scale power plants utilizing coal. This paper reports on the development of a highly efficient, small-scale SOFC power system operating on methane. The system uses adiabatic steam reforming of methane and anode gas recirculation to achieve high net electrical efficiency. The heat and water required for the endothermic reforming reaction are provided by the recirculated anode gas emerging from the SOFC stack. Although the single-pass fuel utilization is only about 55%, because of the anode gas recirculation the overall fuel utilization is up to 93%. The demonstrated system achieved net power output of 1650–2150 W with a maximum net LHV efficiency of 0.566 at 1720 W. Overall system efficiency could be further improved to over 0.60 with use of properly sized blowers.

1. Introduction

1.1. Efficiency of small-scale SOFC power systems

A critical distinction between fuel cell technologies and other energy conversion devices, such as internal combustion engines, is that fuel cell efficiency is not Carnot-limited and fuel cells can achieve relatively high conversion efficiencies at smaller scale operation. Of the available fuel cell technologies, solid oxide fuel cell (SOFC) technology offers the highest electrical conversion efficiencies [1]. In this paper, power system "net efficiency" is defined as the direct current (DC) power produced in excess of that required to support system balance-of-plant loads (e.g., blowers and pumps) divided by the rate of chemical energy supplied in the fuel as measured by the fuel's lower heating value (LHV) enthalpy. System "gross efficiency" refers to the total DC power produced by the SOFC (i.e., no subtraction of balance-of-plant loads) divided by the rate at which fuel LHV energy is supplied.

Since as far back as the late 1990s, there has existed the perception that small-scale (1–10 kW) power systems based on SOFCs alone could not achieve electrical conversion efficiencies of 0.5 or higher. In 1997, Williams [2] published a figure (his Fig. 4) showing efficiencies of fuel cell power systems between 0.3 and 0.4 at the 20 kW power level and trending downward toward less than 0.3 at 1 kW. In 2001, Hassmann [3] published a figure (his Fig. 4) showing efficiency of SOFC power plants decreasing below 0.5 as the power output decreased below 100 kW. A similar figure (Fig. 8-69) appeared in the 2002 edition of the Fuel Cell Handbook [4]. Also in 2002, Bornemann [5] included a figure in which the efficiency of SOFC systems decreased from ~0.4 at 10 kW down to ~0.3 at 1 kW. In 2004, Rukes and Taud [6] published a figure (their Fig. 2) that was very similar to that of Hassmann. As late as 2010, Tomida et al. [7] published a figure showing the efficiencies of small-scale SOFC systems at about 0.45. It is unclear where this perception originated. Most of these publications were focused on discussing the very high efficiencies of large-scale SOFC–gas turbine hybrid power systems. However, in the rush to make that point they gave stand-alone, small-scale SOFC systems too little credit for their ability to achieve high net efficiencies.

The goal of this paper is to describe our demonstration of a highly efficient, small scale (~2 kW) SOFC system that can be readily scaled for a 100–250 kW natural gas fuel distributed generation application. Our system achieves high net efficiency by utilizing steam reforming and anode gas recirculation. System scalability is enabled by using external or adiabatic reforming instead of internal reforming. Details of these technologies and their impacts on the SOFC system are presented in the following sections.

* Corresponding author. Tel.: +1 509 375 2145; fax: +1 509 375 2186.
E-mail addresses: michael.powell@pnnl.gov (M. Powell), k.meinhardt@pnnl.gov (K. Meinhardt), Vincent.Sprenkle@pnnl.gov (V. Sprenkle), larry.chick@pnnl.gov (L. Chick), gary.mcvay@pnnl.gov (G. McVay).

0378-7753/$ – see front matter © 2012 Elsevier B.V. All rights reserved.
doi:10.1016/j.jpowsour.2012.01.098

1.2. Steam reforming versus partial oxidation

A wide variety of system designs have been reported for SOFC-based power systems. The largest influence on overall efficiency is the type of fuel-reforming approach chosen for the system. Systems using partial oxidation (POx) reforming tend to have efficiencies ranging from about 0.25 [8,9] to about 0.4 [10]. Steam reforming, by contrast, gives substantially higher system performance when used with an SOFC stack, because some of the "waste heat" from the stack is converted into increased chemical energy in the reformate. Eq. (1) shows the steam reforming reaction for methane:

$$CH_4 + H_2O + \text{heat} \rightarrow CO + 3H_2 \quad (1)$$

The LHV of methane is 802 kJ mol^{-1}, whereas the LHV of the reaction products (reformate) is 1028 kJ mol^{-1}, which is an energy content increase of 28%. In contrast, Eq. (2) represents POx reformation of methane:

$$CH_4 + (1/2)O_2 \rightarrow CO + 2H_2 + \text{heat} \quad (2)$$

In this case the LHV of the POx reformate is 780 kJ mol^{-1}, which is 32% less than that of the steam reformate. The penalty for POx reformation of the higher hydrocarbons is worse yet, yielding approximately 45% less energy for POx reformate versus steam reforming of dodecane. Mai et al. [10] actually ran the same stack on both catalytic partial oxidation (CPOx) reforming and steam reforming of natural gas. The CPOx system attained 0.40 net LHV efficiency, while the system using steam reforming attained 0.57. The next section is focused on reports of actual demonstrations of SOFC systems that incorporate planar SOFCs and steam reforming of methane.

1.3. Performance of demonstrated SOFC power systems using steam reforming

Payne et al. [11] reported on a 1.5 kW alternating current (AC) co-generation system running on natural gas. The system uses internal (on-stack) reforming of desulfurized and "pre-reformed" natural gas. Based on details in a previous paper [12], the pre-reforming is an autothermal reaction conducted at 390 °C that reforms only the higher hydrocarbons, mainly ethane and propane, and does not alter the methane. Running at 85% fuel utilization and 0.84 V per cell, the system achieved 0.60 net efficiency based on AC power delivered to the grid. Considering that 130 W was lost in the DC/AC inverter, this means the system achieved an efficiency of 0.65 based on net DC power to the inverter.

Dietrich et al. [13] reported on the demonstration of a 300 W SOFC power system running on propane that used partial oxidation for start-up, but switched to external steam reforming with anode off gas recycle for steady state operation. Their reformer incorporated a catalytic burner that burned the non-recycled off gas to provide the heat required for steam reforming. They demonstrated a net efficiency of 0.41 with the system in steady state mode.

Burke and Carreiro [14] reported on an SOFC power system that incorporates anode recycle and steam reforming of synthetic, sulfur-free liquid hydrocarbons (S-8 and JP-10) and methane. They were not able to conserve and transfer enough heat from the SOFC anode outlet to support endothermic steam reforming of S-8. Thus, they recommended using methane as the fuel, although they do not appear to have conducted any testing on pure methane. We suspect the reason the system reported by Burke and Carreiro could not sustain the external reforming reaction is that it did not have a sufficiently high anode flow.

Halinen et al. [15] reported on an SOFC power system running on natural gas. The fuel was mixed with anode recycle gas and partially reformed (~12%) before passing into the stack where reforming was completed in the stack. Their nominal operating point was at 80% fuel utilization, at which they attained a net efficiency of 0.60. They did not report their anode recycle rate.

Bertoldi et al. [16] reported a test of an SOFC stack running on reformate "85% fuel utilization with single-pass flow configuration" that produced an LHV efficiency of 0.65. No other details were given.

Hayashi et al. [17] demonstrated a 5 kW SOFC system running on natural gas and using a post combustor to heat an external steam reformer. Steam for the reformer was produced in a steam generator. Anode exhaust was not recycled. Single-pass fuel utilization was 75%. This produced a net electrical conversion efficiency of 0.44, after DC conversion to AC power at 0.94 efficiency. We take this to mean the system had a net fuel LHV to DC power conversion efficiency of 0.47. Efficiency was about 0.04 higher at 85% fuel utilization, but they wrote "we determined the (75%) fuel utilization by considering the trade-off between durability and electrical efficiency." At 75% fuel utilization the gross conversion efficiency of the stack was 0.56, but the parasitic power was 950 W, 80% of which was consumed by cathode blowers.

Schimanke et al. [18] stated that steam reforming with anode offgas recycling was not possible at small scale "due to missing availability of required balance-of-plant components." They reported on a demonstration of two serially connected stages, the first being a CPOx reformer feeding an SOFC stack. Fresh methane was mixed into the anode off gas from the first stack, which then entered an external steam reformer. The steam reformate then fed a second SOFC stack. Extra heat was added to the steam reformer via an electrical resistance heater. With both stages operating at 80% fuel utilization a net efficiency of 0.56 was achieved.

1.4. Internal versus external steam reforming

There are arguments both for and against the use of internal versus external steam reforming. Payne et al. [11] wrote that the advantages of internal methane reforming over external reforming include (1) lower air flow required to cool the stack due to the cooling from the endothermic steam reforming reaction, (2) less heat loss due to a more compact system, and (3) increased hydrogen yield. They explain this third effect is due to hydrogen being removed by reaction with oxygen emerging from the electrolyte and steam production from the same reaction both forcing the reforming reaction toward the product side and increasing the "maximum fuel utilization that the stack can safely operate at."

In this paper we report on an SOFC power system using external steam reforming, where the anode exit gas is recirculated and the heat and steam required for the endothermic reforming reaction are provided by the anode gas exiting the SOFC stack. We refer to this as *adiabatic* steam reforming, because external heat sources, such as a combustor or an electric-resistance heater, are not necessary to support the reaction. Although the single-pass fuel utilization in the SOFC is only about 55%, the overall fuel utilization is up to 93% due to anode gas recirculation. The anode gas flow rate is relatively high in order to transfer enough heat to the steam reformer to support the endothermic reaction. As a result, about 50% of the stack cooling is through the anode loop.

We designed our system around external steam reforming to avoid thermal quenching of the leading edge of the stack [19], which increases gradients of temperature and current density. This leading-edge stack quenching results from the fact that the kinetics of steam reforming over SOFC anodes is much faster than the electrochemical reactions [20]. The magnitude of the predicted thermal and current density gradients depends heavily upon the parameters used by the modeler. Modeling by Iwai et al. [21] shows that, with internal reforming the current density can increase by as much as a factor of ten from leading edge to the maximum, which occurred at about 85% of the length of the cell. Li et al. [22] also predicted a ten-fold range of current density in a cross-flow

stack with internal reforming. Most researchers predict current density gradients in the range of factors of two or three [23–26]. The lowest predicted current density gradient factor found was only 30% [27]. However, those who compare internal versus external reforming consistently find internal reforming produces larger gradients in the stack than does external reforming [24,28,29]. Due to the quenching of the SOFC leading edge, internal reforming effectively substitutes expensive SOFC area for a comparatively *inexpensive* external reformer. Another concern is the introduction of internal stress due to the increased thermal gradients introduced by internal reforming [29–33]. Reducing thermal gradients within the active cell area is expected to improve SOFC robustness and reliability.

2. Experimental

The layout and operation of our integrated SOFC power system is described in Section 2.1. Test methods, system control, and instrumentation are described in Section 2.2.

2.1. System description

A simplified configuration diagram of the integrated test system is provided in Fig. 1. Stream numbers referred to in the text below are indicated by the circled numbers in Fig. 1. To facilitate understanding of the temperature, pressure, and composition changes in the system, we have included Tables 1 and 2, which provide sample experimental data for each stream. The data in Tables 1 and 2 are for one of the high-efficiency/low-power test conditions (test 12 in Table 3). Nitrogen present in the anode gas was due to leakage from the cathode gas into the anode gas. This leakage is discussed further in Section 3.

The integrated test system includes four SOFC stacks connected in parallel with respect to the anode and cathode gas flows. Sulfur-free, >99.99% pure methane from gas cylinders (stream #1) is added to the circulating anode gas flow (stream #2) just upstream of the steam reformer. As the mixture of stack anode exit gas and CH_4 (stream #3) contacts the reforming catalyst, the fuel molecules are reformed to CO, CO_2, CH_4, H_2, and H_2O in proportions that depend both on the temperature and on the ratio of gas flow to CH_4 flow. The reformate mixture (stream #4) then flows through the anode recuperator where it cools to approximately 200 °C. Some heat is intentionally lost to the surroundings as the anode gas continues to the anode blower where the approximately 150 °C gas is pressurized and returned to the anode recuperator (stream #7). Cooling the anode gas to 150 °C is necessitated by the allowable inlet temperature for the anode recycle blower. The anode gas is heated by the anode recuperator and then fed to the SOFC stacks, thereby completing the anode-gas recycle loop.

The anode loop comprises four SOFC stacks, one steam reformer, one anode recuperator, and one anode blower. Flow to the four stacks is distributed using a manifold made from 3.8-cm-dia. tubing. The pressure drop in the anode channels of the SOFCs is higher than that of the manifold and this difference ensures near uniform distribution of fuel gas to each of the stacks.

Oxidation byproducts (CO_2 and H_2O) are removed from the anode gas loop via a purge-gas stream (stream #9) that splits from the main anode flow just upstream of the CH_4-addition point. The purge gas flows through the anode recuperator as a separate stream and then through a condenser, which removes most of the water. The remaining purge gas (stream #11) was vented in our tests, but in combined-heat-and-power applications it could be combusted to extract its available chemical energy.

Anode gas is recycled at a rate determined by the anode blower speed. Recycle rates in our tests varied from 83 to 90%. Recycle rate is defined as the percentage of SOFC anode exit gas that continues toward the adiabatic reformer rather than exiting by the purge-gas stream. Flow rate of the purge-gas stream was not actively controlled; as gas accumulates within the fixed volume of the anode flow loop, the increasing pressure results in increased purge-gas flow out of the system.

Centrifugal blowers force ambient air (stream #12) through the cathode recuperators, which heat the air to between 600 and 700 °C before it enters the cathode channels of the SOFC stacks. The data in Table 1 indicate relatively low recuperator exit temperatures (approximately 600 °C) and this is due to reduced recuperator

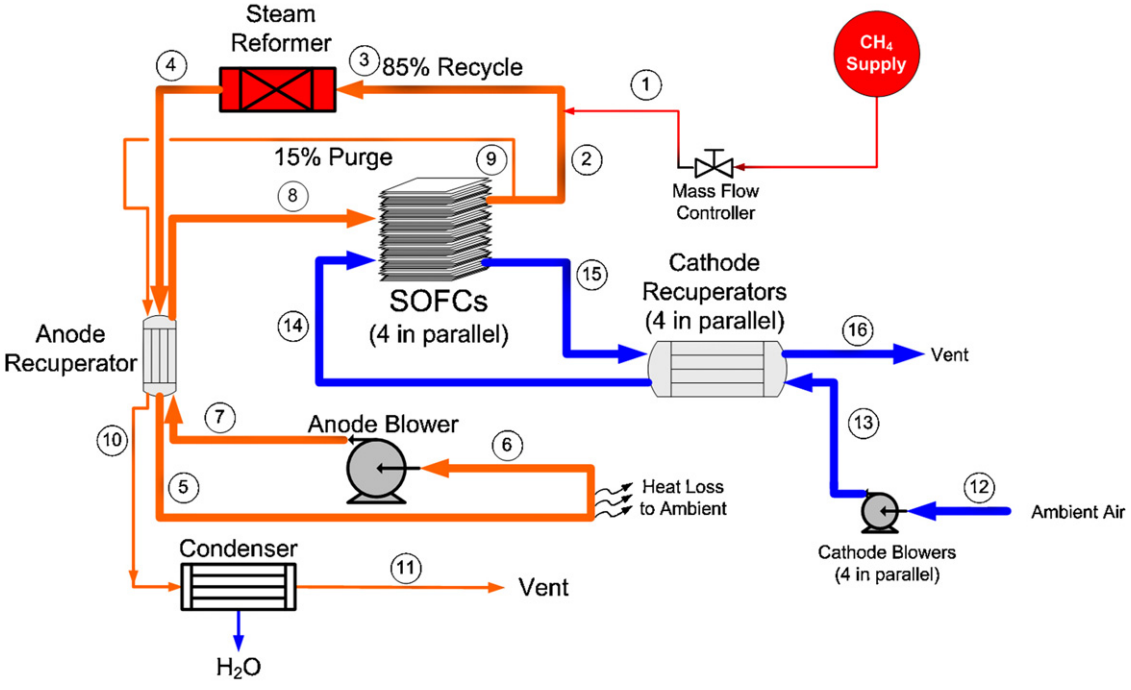

Fig. 1. Power system configuration diagram.

Table 1
Example stream conditions for operation at 85% recycle, U_f = 93%, 1885 W gross output, 1717 W net output.

Stream #	Temperature (C)	Gauge pressure (kPa)	Flow rate (mol min^{-1})	Estimated enthalpy[a] (W)
1	25	1.3	0.23	−280
2	765	1.3	3.5	−12,990
3	710	1.3	3.7	−13,270
4	530	1.1	4.0	−13,250
5	200	0.38	4.0	−14,090
6	145	0.38	4.0	−14,230
7	170	4.4	4.0	−14,160
8	540	3.3	4.0	−13,220
9	765	1.3	0.64	−2370
10	200	0.38	0.64	−2610
11	25	0.0	0.64	−2930
12	25	0.0	3.1	0
13	35	1.5	3.1	15
14	600	1.1	3.1	910
15	750	0.38	2.7	1000
16	110	0.0	2.7	110

[a] Enthalpy values are calculated based on the measured temperature, pressure, flow rate, and composition of each stream. Reference conditions are 1 atm and 25 °C.

Table 2
Stream compositions for operation at 85% recycle, U_f = 93%, 1885 W gross output, 1717 W net output.

Stream #	CO_2 (% mol.)	CO (% mol.)	CH_4 (% mol.)	H_2 (% mol.)	H_2O (% mol.)	N_2 (% mol.)	O_2 (% mol.)	Argon (% mol.)
1	0	0	100	0	0	0	0	0
2	29	2.6	0	5.6	57	6.5	0	0
3	27	2.5	6.1	5.2	53	6.2	0	0
4	28	3.1	1.8	19	42	5.7	0	0
5	28	3.1	1.8	19	42	5.7	0	0
6	28	3.1	1.8	19	42	5.7	0	0
7	28	3.1	1.8	19	42	5.7	0	0
8	28	3.1	1.8	19	42	5.7	0	0
9	29	2.6	0	5.6	57	6.5	0	0
10	29	2.6	0	5.6	57	6.5	0	0
11	29	2.6	0	5.6	57	6.5	0	0
12	0	0	0	0	0	78	21	1
13	0	0	0	0	0	78	21	1
14	0	0	0	0	0	78	21	1
15	0	0	0	0	0	90	9.2	1.2
16	0	0	0	0	0	90	9.2	1.2

Table 3
Integrated SOFC power system performance data.

Test #	CH_4 flow (mol min^{-1})	Gross power (W)	Blower power (W)	Recycle rate (%)	U_f (%)	Gross efficiency	Net efficiency
1	0.308	2400	250	83	86	0.585	0.523
2	0.308	2380	300	86	86	0.579	0.506
3	0.308	2480	310	85	93	0.605	0.529
4	0.286	2330	300	87	93	0.611	0.533
5	0.275	2260	290	86	93	0.615	0.537
6	0.265	2190	260	86	93	0.619	0.545
7	0.308	2390	280	83	86	0.582	0.515
8	0.255	2110	240	86	93	0.621	0.551
9	0.244	2030	240	85	93	0.623	0.549
10	0.233	1950	220	86	93	0.626	0.557
11	0.224	1870	200	86	93	0.627	0.558
12	0.228	1880	170	85	91	0.621	0.566
13	0.343	2600	320	84	86	0.569	0.499
14	0.331	2580	330	84	89	0.585	0.510
15	0.319	2540	360	86	93	0.596	0.512
16	0.331	2560	400	87	89	0.581	0.490
17	0.343	2590	390	86	86	0.566	0.482
18	0.319	2520	410	87	93	0.593	0.497
19	0.308	2380	280	85	86	0.578	0.509
20	0.297	2350	290	86	89	0.594	0.521
21	0.287	2320	310	86	93	0.605	0.524
22	0.308	2360	340	89	86	0.574	0.490
23	0.297	2340	350	90	89	0.591	0.503
24	0.287	2310	350	90	93	0.604	0.511

performance at the low anode and cathode flow rates used for the high-efficiency tests.

A fraction of the oxygen in the cathode gas is removed by the fuel cell electrochemical reaction and the remaining gas (stream #15) flows back through the recuperators before it is vented to ambient at a temperature of about 100 °C (stream #16). Each SOFC stack has its own cathode air blower and recuperator to allow accurate control of the maximum temperature within each stack. Because each

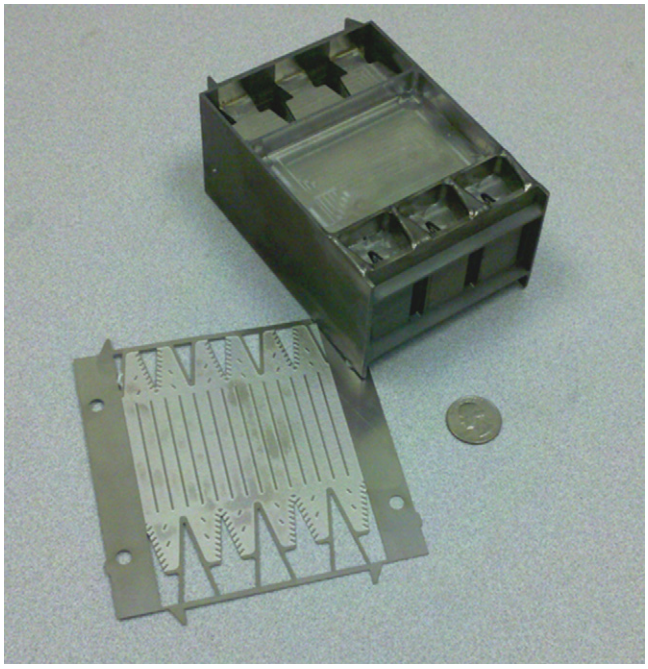

Fig. 2. Microchannel heat exchanger and photochemically etched shim.

of the four SOFC stacks has a slightly different thermal environment, each stack requires a different cathode air flow to maintain a stable operating temperature.

The anode and cathode recuperators are microchannel devices made using a combination of photochemical etching and diffusion bonding. Sub-millimeter-scale flow paths are etched into metal shims, which are stacked and fused together by high-temperature diffusion bonding in a vacuum furnace. Microchannel heat exchanger architecture yields compact heat exchangers with high thermal effectiveness and low pressure drop [34]. Fig. 2 shows a typical microchannel heat exchanger alongside some of the etched shims used to build the device.

The microchannel heat exchangers in the integrated test system provided a typical thermal effectiveness of up to 0.90 and a per-pass pressure loss of 0.5–1.5 kPa. High thermal effectiveness reduces exergy loss, which allows more of the generated heat to be used for steam reforming of the fuel. Low pressure loss reduces the parasitic power demands of the anode and cathode blowers, which results in improved net system efficiency. Power consumed by the blowers represents the principal parasitic power loss, so reducing the pressure loss in system components to minimal levels is essential for maintaining high system net efficiency.

The adiabatic steam reformer is a 10-l canister filled with a noble-metal-based reforming catalyst deposited on a fecralloy foam support acquired from Porvair (Hendersonville, North Carolina). The metal foam has a pore density of 60 pores per inch and a 95% void volume. The metal-foam catalyst support provides high catalyst contact area and low pressure drop. Pressure loss from the steam reformer is less than 0.1 kPa. The high-activity steam reforming catalyst was developed by Battelle (Columbus, Ohio) and its composition is proprietary.

The anode recycle blower is a model 3BA72100MAG from AirTech West (Novato, California). This regenerative blower is designed to tolerate gas inlet temperatures of up to 200 °C. Blower capacity is larger than required for this test by about a factor of four. We opted to use this excess-capacity blower for the testing to allow for greater flexibility in system operation and to avoid the cost of a custom blower designed for high inlet temperatures. Cathode air was supplied using four model 150193 centrifugal blowers from Ametek Technical and Industrial Products (Kent, Ohio). One blower was used for each stack to allow independent control of stack temperatures. Four cathode recuperators are used to ensure each stack receives its own, independently controlled air supply. The cathode blower capacities were larger than required by about a factor of five. The cathode blowers were intentionally oversized to allow sufficient operating margin even when the system was operated in a high-power mode where stack voltages are reduced and significantly more stack cooling is required than for the high-efficiency conditions described in this paper.

The four SOFC stacks, provided by Delphi Corp., were each composed of 30 cells with planar, anode-supported architecture. Each cell has an active area of 105 cm^2. The cells have lanthanum–strontium–cobalt–iron cathodes (~30 μm), a ceria based interlayer (~4 μm), an 8 mole% yttria stabilized zirconia (YSZ) electrolyte (~10 μm) a nickel–YSZ active anode (~10 μm) and a nickel–YSZ bulk anode (~500 μm) [8].

2.2. Test methods, system control, and instrumentation

The locations of all process monitoring instruments are shown in Fig. 3. Temperature measurements used type K thermocouples. For each steady-state test condition, gas samples were collected from each of the locations indicated in Fig. 3. These samples were analyzed using an Agilent Technologies (Santa Clara, California) model 3000A Micro gas chromatograph equipped with molecular sieve 5A, Plot U, and OV-1 columns.

Methane was supplied by compressed gas cylinders from Matheson Gas Products (Newark, California). The CH_4 is sulfur-free and has a purity of >99.99%. The CH_4 feed rate was controlled with a 0–0.6 mol min^{-1} model 5851i mass flow controller from Brooks Instrument (Hatfield, Pennsylvania). The mass flow controller accuracy was verified before and after testing and determined to be ±0.003 mol min^{-1}. Flow accuracy was determined with a DryCal gas flow calibrator from Bios International Corporation (Butler, New Jersey).

A combination of gauge and differential pressure transducers were used to allow accurate characterization of pressure throughout the system. Omega model PX-409 differential pressure transducers were used with ranges selected according to the expected system pressure at each location. The accuracy of these sensors for the ranges selected is ±75 Pa or better. For gauge pressure measurement, one side of the differential pressure transducer was opened to atmosphere. All system tests took place in an indoor lab with ambient temperature controlled to 20 ± 2 °C.

Each of the four SOFC stacks was instrumented with internal thermocouples at the expected location of maximum stack temperature (near the gas exit region of cell 15 in the 30-cell stacks). Voltage leads were also installed on each pair of cells such that for each 30-cell stack a total of 15 voltage measurements were made and recorded by the system controller. Cell voltage measurements were used to identify conditions where one or more cells were receiving insufficient fuel or oxygen supply.

Cathode gas flow rate was measured using model 730 air mass meters from Sierra Instruments (Monterey, California). Expected accuracy for the flow meters is ±0.2 mol min^{-1}.

Stack temperatures were monitored with type K thermocouples installed inside each stack. An automated feedback control system was used to maintain the maximum stack thermocouple readings at approximately 790 ± 2 °C. The control system increases or decreases the speed of the cathode blower for each stack as necessary to achieve the target operating temperature.

Anode gas flow rate was calculated from the measured inlet-to-outlet differential pressure of the SOFC stack anode channels. Before testing, the relationship between anode-channel pressure drop and room-temperature nitrogen flow rate was determined.

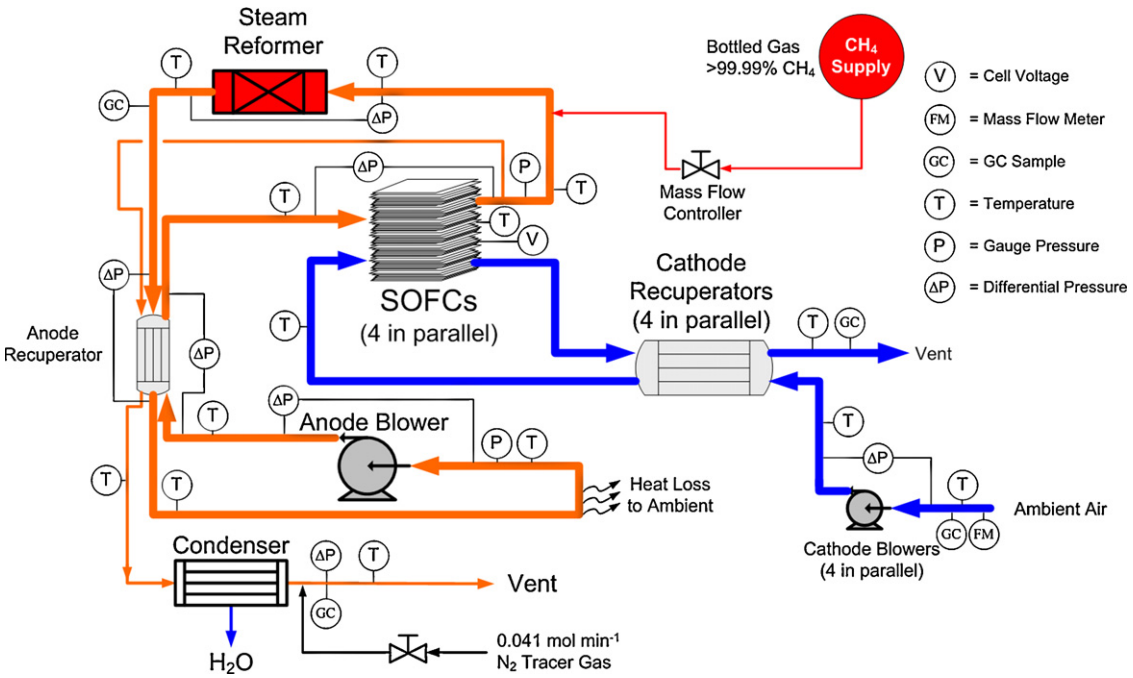

Fig. 3. System instrumentation and gas sampling locations.

These data were used to predict the expected relationship between anode-gas flow and pressure drop during system operation. Corrections for temperature, pressure, and composition were applied using a Reynolds number/friction factor approach. The stack feed and exit gas compositions were determined by gas chromatography. The measured compositions agree well with expectations based on chemical process modeling for each set of test conditions and this agreement provides added confidence in the accuracy of our approach for quantifying the anode gas flow rate.

Purge gas flow rate was measured using an inert tracer gas (nitrogen) periodically added to the purge-gas flow at a fixed rate of 0.041 ± 0.001 mol min^{-1} by a mass flow controller. Gas chromatography analysis of the purge gas composition with and without tracer gas addition was used to directly calculate the purge gas flow rate using a mass balance approach. The purge gas composition was measured downstream of the condenser, so most of the water had already been removed. The water condensation rate was determined by continuous collection of the water in a 10-l carboy resting upon a digital scale.

Anode gas recycle rate was calculated based on the anode gas flow rate, which was estimated from the anode channel pressure drop, and the total purge gas flow. The total purge flow was the sum of the rate of water collected in the condenser and the dry purge gas flow determined by gas chromatography. The uncertainty in the total purge gas flow rate (~3%) results in a ±0.5% absolute uncertainty (e.g., $85 \pm 0.5\%$) in the recycle rate estimates. Accordingly, recycle rate data are reported to the nearest whole percentage. Adjustments to the anode gas recycle rate were made by increasing or decreasing the anode blower speed. Anode recycle rates were varied between 83% and 90%.

Electric power generated by the SOFC stacks was controlled, measured, and dissipated using a 4 kW-capacity, model PLA4K-120-600 electronic load bank from Amrel Corp. (El Monte, California). Power consumed by the anode and cathode blowers was measured using a current-transformer-based ammeter surrounding the power supply wires for each blower.

Estimates for overall fuel utilization (U_f) were made based on the CH_4 feed rate and the purge gas flow rate and composition. The LHV for the purge gas is subtracted from the CH_4 feed LHV to determine the rate of fuel energy consumption in the system. This consumption rate is divided by the CH_4 feed LHV to determine the percentage of overall fuel utilization. Overall fuel utilization was adjusted using the load bank, which was operated in a constant-current mode. Increases in the current drawn by the load bank result in increased U_f.

Gross system efficiency was calculated by dividing the gross power generated (i.e., the power dissipated by the load bank) by the LHV rate of chemical energy supplied by the CH_4 feed stream. Net system efficiency was calculated by subtracting the power demands of the anode and cathode blowers from the gross power before dividing by the LHV of the CH_4 feed stream.

For each test condition reported here, the system was allowed to reach a chemically and thermally stable condition. A minimum of 0.5 h was allowed for system stabilization at each condition. In cases where a relatively large change was made in system power levels, 1.0 h or more was allowed for stabilization. Total system test time was 98 h on sulfur-free methane.

Each test involved adjusting the anode blower speed, CH_4 feed rate, and load-bank current draw to achieve the desired anode recycle rate and system gross output power. The system was then allowed to stabilize for at least 0.5 h. During this period, the cathode blower speeds were automatically adjusted by the system controller to maintain a target maximum temperature in each SOFC stack of about $790 \pm 2\,^{\circ}$C. After the stabilization period, measurements of the input electric power for the anode and cathode blowers were made and gas samples were collected for analysis by gas chromatography. During the tests, the system controller recorded all temperature, pressure, flow rate, electrical load, and condensate production rate data at a frequency of 1 Hz.

When the goal of the test was to maximize U_f, the load-bank current was slowly increased while monitoring stack cell voltages (recycle rate and CH_4 addition rate were held constant). Generally, when U_f exceeded 93%, a sharp decrease in one or more cell voltages was observed. This decrease indicates insufficient fuel supply to the cells with the lowered voltages. The load-bank current was then decreased to allow recovery of the voltages and the system was allowed to stabilize for at least 0.5 h before measurement of gas compositions and blower power demands.

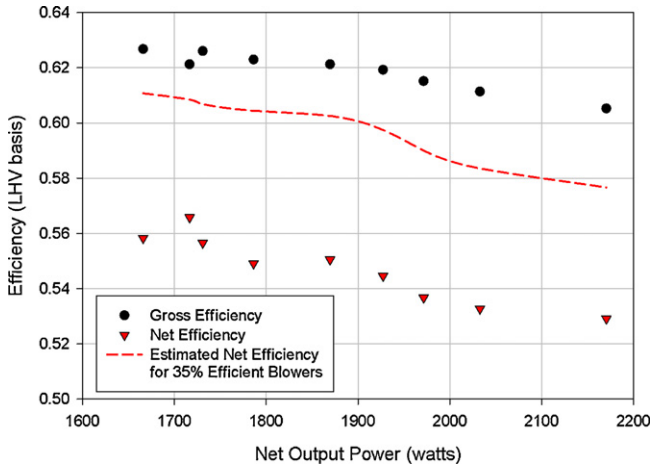

Fig. 4. System efficiency vs. output power.

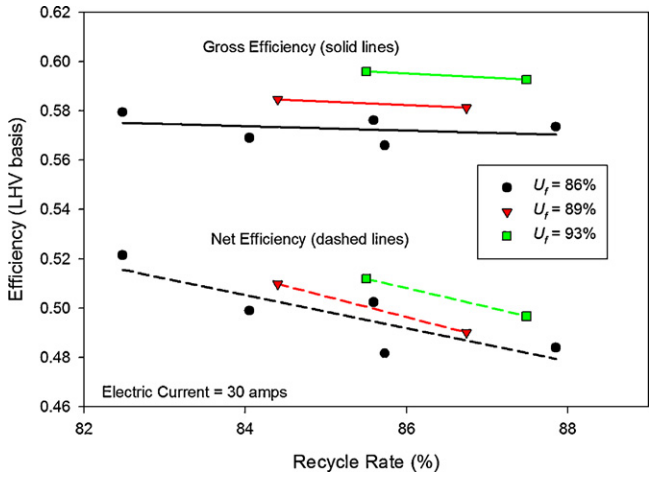

Fig. 5. System efficiency vs. recycle rate and overall fuel utilization. Lines shown on plot are intended to aid the eye and are not necessarily indicative of trends.

3. Results and discussion

Steady-state system performance data are summarized in Table 3. Each row in Table 3 represents one steady-state test and the tests are listed in the order we conducted them. Stability was demonstrated periodically throughout the testing by placing the system in the same stable operating condition and verifying there had been no significant change in gross output power (see tests 1, 2, 7, and 19).

SOFC gross output power varied between 1870 and 2600 W. Net power (i.e., gross power minus the sum of all blower power demands) ranged from 1670 to 2280 W. For each steady-state power level measurement, recycle rate and single-pass fuel utilization were adjusted in an effort to maximize system-level net efficiency. Fig. 4 shows the variation of gross and net LHV efficiency with net output power. The data shown in Fig. 4 were collected at U_f between 91% and 93%.

At net output power levels of up to 1900 W, the gross LHV efficiency exceeds 0.62 and the net LHV efficiency exceeds 0.545. Peak net LHV efficiency of 0.567 was obtained at 1720 W net output power. With increasing net output power, the gross LHV efficiency decreases due to the decrease in stack voltage that occurs as power density increases. The net LHV efficiency decreases because of the combined effect of decreasing gross efficiency and the increase in parasitic power demands from the anode and cathode blowers, which must flow more gas against increasing pressure as system output power is increased.

Fig. 4 includes a dashed line indicating the net efficiency expected from the system if the existing, over-sized blowers were replaced with blowers sized specifically for the flow rates and pressure drops observed in the testing. Blower efficiencies of 35% were assumed for the purpose of generating this estimate. With the 35%-efficient blowers, the system net efficiency is expected to reach 0.61 at 1700 W net output. During our tests, the anode blower efficiency was typically 8% and the average cathode blower efficiency was 12–15%.

Power system tests included varying both the recycle rate and the overall fuel utilization. Recycle rates varied from 83% to 90%. Overall fuel utilization, U_f, varied from 86% to 93%. Overall fuel utilization quantifies the fraction of steam-reformed methane that is oxidized in the fuel cell. Higher U_f implies more complete consumption of fuel. Fig. 5 shows the effect of changes in recycle rate and U_f on the net and gross LHV efficiency at a constant current of 30 A. The lines included on the Fig. 5 plot are intended to aid the eye and distinguish between gross and net efficiency values. Because the lines for U_f = 89% and 93% are based on only two data points, they are not necessarily representative of the actual trends in system performance.

For constant U_f, increasing recycle rate results in a slight decrease in gross LHV efficiency because higher recycle rates imply more dilute fuel fed to the SOFC stacks. With increased recycle rate, a greater fraction of the anode feed gas is composed of CO_2 and H_2O rather than H_2, CO, and CH_4. The effect of recycle rate on net LHV efficiency is more significant because the reduction in fuel concentration is coupled with an increase in anode blower power demand. Use of a more efficient anode blower would make the net LHV efficiency less sensitive to changes in recycle rate.

Increases in U_f result in significant increases in both gross and net system efficiency. As U_f increases, less fuel exits the recycled anode gas via the purge-gas stream. The U_f cannot be increased much beyond 93% in our system. Distribution of fuel gas to the cells in the stacks is not perfectly uniform, yet because the cells are all connected electrically in series, they all have the same electric current and the same rate of fuel consumption. Cells that receive less than the average flow of anode feed gas can, in effect, run out of fuel. This is indicated by a reduction in cell voltage for those particular cells while cells with more fuel feed continue operating at higher voltages. In our system, we increased U_f to 93% and could run stably in that condition. Attempts at operation with higher U_f resulted in sharp reductions in some of the cell voltages. Consequently, tests with U_f adjusted to ~93% represent the maximum efficiency for our system.

In combined heat and power applications, operation at lower U_f is not necessarily problematic because the fuel gas exiting in the purge-gas stream can be combusted to provide useful heat. In our efficiency estimates provided here we are not taking credit for any heating energy that might be extracted from the purge-gas stream.

As mentioned in Section 2, leakage of cathode gas into the anode gas was observed during these tests. The presence of nitrogen in the anode purge gas is explained by cross-flow leakage of cathode gas into the anode gas. We are continuing to investigate the cause of this leakage. Possible leak locations include the gasketed connections between the stacks and the inlet manifolds as well as inside the stacks. Note that because of the accumulating effects of anode-gas recycle on inert gases such as nitrogen, even a relatively small leak will result in relatively high steady-state nitrogen concentrations. Based on the nitrogen flow rate in the purge gas, the amount of oxygen leaking into the anode gas was typically less than 3% of the oxygen transported electrochemically in the stack, so the impact of the cathode-to-anode leakage on system efficiency is relatively minor. Once the source of the leak is

identified and corrected, though, there will be a slight increase in system efficiency.

4. Conclusions

We have shown that it is possible to achieve highly efficient SOFC power systems utilizing adiabatic, external steam reforming. The heat and steam required for reformation of the methane was provided by the circulating anode exhaust gas. Adiabatic steam reforming of methane is the preferred option for larger scale SOFC systems since the thermal gradients in the cell are minimized when compared to internal reformation. The demonstrated system used adiabatic steam reforming of methane along with anode gas recirculation to achieve a maximum net LHV efficiency of 0.566 at 1720 W. Overall system efficiency could be further improved to over 0.60 with use of properly sized blowers.

Acknowledgement

The authors wish to thank the U.S. Department of Energy Office of Fossil Energy for supporting this work.

References

[1] A. Elgowainy, M. Wang, Fuel Cycle Comparison of Distributed Power Generation Technologies, 2008, ANL/ESD/08-4.
[2] M. Williams, SOFC V, Electrochemical Society Proceedings, PV 97-40, 1997, pp. 3–11.
[3] K. Hassmann, Fuel Cells 1 (1) (2001) 78–84.
[4] Fuel Cell Handbook, 6th ed., 2002, DOE/NETL-2002/1179.
[5] H. Bornemann, Proceedings of the 2nd DOE/UN Workshop and International Conference on Hybrid Power Systems, 2002.
[6] B. Rukes, R. Taud, Energy 29 (2004) 1853–1874.
[7] K. Tomida, M. Nishiura, S. Koga, K. Miyamoto, Y. Teramoto, S. Yoshida, N. Matake, S. Suemori, T. Kabata, Y. Ando, Y. Kobayashi, Fuel Cell Seminar, 2010.
[8] S. Mukerjee, K. Haltiner, R. Kerr, J.Y. Kim, V. Sprenkle, SOFC XII, Electrochemical Society Transactions, vol. 35(1), 2011, pp. 139–146.
[9] S. Reuber, M. Schneider, M. Stelter, A. Michaelis, SOFC XII, Electrochemical Society Transactions, vol. 35(1), 2011, pp. 251–258.
[10] A. Mai, B. Iwanschitz, U. Weissen, R. Denzler, D. Haberstock, V. Nerlich, A. Schuler, SOFC XII, Electrochemical Society Transactions, vol. 35(1), 2011, pp. 87–95.
[11] R. Payne, J. Love, M. Kah, SOFC XI, Electrochemical Society Transactions, vol. 25(2), 2009, pp. 231–239.
[12] K. Foger, B. Godfrey, Proceedings of Fuel Cell 2000, Lucerne, Switzerland, July 10–14, 2000, p. 185.
[13] R. Dietrich, J. Oelze, A. Lindermeir, C. Spitta, M. Steffen, T. Kuster, S. Chen, C. Schlitzberger, R. Leithner, J. Power Sources 196 (2011) 7152–7160.
[14] A. Burke, L. Carreiro, SOFC XII, Electrochemical Society Transactions, vol. 35(1), 2011, pp. 2815–2823.
[15] M. Halinen, M. Rautanen, J. Saarinen, J. Pennanen, A. Pohjoranta, J. Kiviaho, M. Pastula, B. Nuttall, C. Rankinb, B. Borglum, SOFC XII, ECS Transactions, vol. 35(1), 2011, pp. 113–120.
[16] M. Bertoldi, O. Bucheli, S. Modena, D. Larrain, A. Ravagni, SOFC XII, ECS Transactions, vol. 35(1), 2011, pp. 127–138.
[17] K. Hayashi, A. Miyasaka, N. Katou, Y. Yoshida, H. Arai, M. Hirakawa, H. Uwani, S. Kashima, H. Orisima, S. Kurachi, A. Matsui, K. Katsurayama, E. Tohma, SOFC XII, ECS Transactions, vol. 35(1), 2011, pp. 121–126.
[18] D. Schimanke, O. Posdziech, B. Mai, S. Kluge, T. Strohbach, C. Wunderlich, SOFC XII, ECS Transactions, vol. 35(1), 2011, pp. 231–242.
[19] T. Ho, P. Kosinski, A. Hoffman, A. Vik, Int. J. Hydrogen Energy 34 (8) (2009) 3488–3499.
[20] D. Mogensen, J.-D. Grunwaldt, P.V. Hendriksen, K. Dam-Johansen, J.U. Nielsen, J. Power Sources 196 (2011) 25–38.
[21] H. Iwai, Y. Yamamoto, M. Saito, H. Yoshida, Energy 36 (4) (2011) 2225–2234.
[22] J. Li, G. Cao, X. Zhu, H. Tu, J. Power Sources 171 (2) (2007) 585–600.
[23] K. Recknagle, E. Ryan, B. Koeppel, L. Mahoney, M. Khaleel, J. Power sources 195 (19) (2010) 6637–6644.
[24] K. Lai, B. Koeppel, K. Choi, K. Recknagle, X. Sun, L. Chick, V. Korolev, M. Khaleel, J. Power sources 196 (6) (2011) 3204–3222.
[25] C. Bao, Y. Shi, E. Croiset, C. Li, N. Cai, J. Power sources 195 (15) (2010) 4871–4892.
[26] C. Colpan, F. Hamdullahpur, I. Dincer, J. Power Sources 195 (11) (2010) 3579–3589.
[27] T. Ho, P. Kosinski, A. Hoffman, A. Vik, J. Power Sources 195 (19) (2010) 6764–6773.
[28] M. Andersson, H. Paradis, J. Yuan, B. Sunden, J. Fuel Cell Sci. Technol. 8 (3) (2011), Article # 031013.
[29] A. Nakajo, Z. Wuillemin, J. Van Herle, D. Favrat, J. Power Sources 193 (1) (2009) 216–226.
[30] M. Boder, R. Dittmeyer, J. Power Sources 155 (2006) 13–22.
[31] J. Klein, S. Georges, Y. Bultel, J. Appl. Electrochem. 40 (5) (2008) 943–954.
[32] A. Nakajo, Z. Wuillemin, J. Van Herle, D. Favrat, J. Power Sources 193 (1) (2009) 203–215.
[33] B. Shaffer, J. Brouwer, Proceedings of the 7th International Conference on Fuel Cell Science, Engineering and Technology, ASME, 2009, pp. 603–616.
[34] R. Wegeng, C. Call, M. Drost, Proceedings of the AIChE 1996 Spring National Meeting, New Orleans, Louisiana, 1996.